Synthesis, Structural, and Magnetic Properties of $Ba_3(Zn_xMg_{1-x})_2Fe_{24}O_{41}$ Z-Type Hexaferrites

E.S. Al-Hwaitat[a], M.A. Hussein[a], I. Bsoul[b], R.A. Buqain[c] and S.H. Mahmood[a,*]

[a]Department of Physics, The University of Jordan, Amman 11942, Jordan

[b]Department of Physics, Al al-Bayt University, Mafraq 13040, Jordan

[c]Cell thereby centre, The University of Jordan, Amman 11942, Jordan

(Received July 26, 2019; in final form August 9, 2019)

This article is concerned with the synthesis of high-quality (Mg, Zn)$_2$Z hexaferrites. A series of the ferrites $Ba_3(Zn_xMg_{1-x})_2Fe_{24}O_{41}$ ($x = 0.5$, 0.7, and 1.0) were prepared by high-energy ball milling and sintering at 1250 °C for 2 h. The structural and magnetic properties of the samples were investigated using X-ray diffraction, scanning electron microscopy, and vibrating sample magnetometer. X-ray diffraction and thermomagnetic studies indicated that the Z-type phase was dominant at $x = 0.5$, and decreased with the increase of x, whereas the fraction of the Y-type hexaferrite increased. The saturation magnetization and initial permeability, however, increased slightly with the increase of x. The coercivity, on the other hand, was in the range 40–54 Oe for all samples, and the magnetocrystalline anisotropy field did not change significantly with increasing x. The FMR frequency estimated from the static magnetic parameters was ≈ 19 GHz for all samples.

DOI: 10.12693/APhysPolA.136.548

PACS/topics: Z-type hexaferrites, structural properties, magnetic properties, initial permeability, FMR frequency

1. Introduction

Hexaferrites are widely used as essential components for a large variety of industrial and technological applications; automotive industry, electronic, telecommunication, data storage and processing, microwave devices, instrumentation, radar technologies, and motor industry [1–7]. Hexaferrites can be classified into six main types: M, Y, Z, W, X, and U, according to different stacking sequences of S, R, and T fundamental structural blocks in their crystal structure [8].

In the hexagonal ferrite family, M-type barium ferrites have been extensively used in permanent magnets and perpendicular recording materials, dominating the permanent magnet world market due to their stability, easy fabrication, availability of raw materials, suitable magnetic properties, and cost effectiveness [9]. Z-type hexaferrites, on the other hand, had attracted attention due to their high initial permeability in frequency regions higher than 300 MHz, excellent electromagnetic properties, and ferromagnetic resonance frequency up to the GHz range. Therefore, these ferrites are considered to be promising materials for multilayer chip inductors (MLCI), phase shifters, and microwave absorbers in high frequency range [10–16]. Synthesis of pure Z-type hexaferrite is a real challenge due to the complexity of its structure, and the progressive transformation through intermediate phases before achieving the final required product [17–19]. Impurity Y and W, as well as other identifiable and unidentifiable phases coexisting with the Z-type phase seem to be inevitable [20, 21].

*corresponding author; e-mail: s.mahmood@ju.edu.jo

The magnetic and dielectric properties of hexaferrites can be controlled by the type and amount of substitution of divalent or trivalent ions [12, 19]. It was reported that the incorporation of divalent metal ions such as Cu^{2+}, Zn^{2+}, Ca^{2+}, Ni^{2+}, and Mn^{2+} in Z-type hexaferrite may improve their properties [12, 20, 22–26]. In a recent study, the effects of the substitution level of Zn^{2+} on the purity and magnetic properties of $Ba_3(Cu_{0.8-x}Zn_xMn_{0.2})_2Fe_{24}O_{41}$ hexaferrite were investigated [27]. In this study, it was demonstrated that intermediate levels of Zn substitution for Cu ($0.2 \leq x \leq 0.6$) was suitable for the production of a highly pure Z-type phase, with increased saturation magnetization, and reduced coercivity and magnetocrystalline anisotropy. Also, the substitution of Zn^{2+} for Co^{2+} in Co_2Z hexaferrite was carried out to improve the initial permeability for multilayer chip inductor applications [14], and reduce the reflectivity for electromagnetic absorption applications [16].

Much interest in Y- and Z-type hexaferrites was also driven by their magneto-electric properties and potential for non-volatile memory elements [28–30]. In particular, magneto-electric effect was observed in $Ba_{0.5}Sr_{1.5}Zn_2Fe_{12}O_{22}$, and $Sr_3Co_2Fe_{24}O_{41}$ hexaferrites. Also, Mg_2Y hexaferrites, as well as effects of Zn substitution for Mg were investigated due to their interesting magneto-electric properties [31] (and references therein). However, up to our knowledge, no serious attempt was made to synthesize and characterize Mg_2Z hexaferrites. In this study, we investigate the effect of Zn^{2+} ion substitution on the structural and magnetic properties of $Ba_3(Zn_xMg_{1-x})_2Fe_{24}O_{41}$ ($x = 0.5$, 0.7, 1.0) hexaferrites. Our study might serve as a step toward the synthesis of Zn doped Mg_2Z-type hexaferrite, and provide essential information on its structural and magnetic properties.

2. Experimental techniques

$Ba_3(Zn_xMg_{1-x})_2Fe_{24}O_{41}$ ($x = 0.5, 0.7, 1.0$) were prepared by high-energy ball milling. Stoichiometric amounts of the starting materials; Fe_2O_3 ZnO, MgO, and $BaCO_3$ were weighed and milled in a planetary ball-mill with a powder to ball ratio of 1:12. Milling was carried out for 16 h at a rotational speed of 250 rpm. The powder mixtures for the samples were compacted into disk-shape pellets of ≈ 1.2 cm diameter and ≈ 2 mm thickness under a force of 50 kN, and sintered at 1250 °C for 2 h in air.

The structure for the different samples was investigated by X-ray diffraction (XRD) using a 7000 X-ray diffractometer, with Cu radiation ($\lambda = 0.154$ nm). XRD diffraction patterns for the samples were recorded over the angular range $20° < 2\theta < 70°$ with scanning step of 0.01° and scan speed of 0.5 deg/min. A powder diffraction software package which includes the standards of international centre of diffraction data (ICDD) was used to identify the observed structural phases. The morphology of the prepared samples was examined using scanning electron microscope (SEM). The magnetic characteristics of the prepared samples were obtained using a vibrating sample magnetometer (VSM).

3. Results and discussion

3.1. XRD results

Figure 1 shows the X- ray diffraction patterns for the $Ba_3(Zn_xMg_{1-x})_2Fe_{24}O_{41}$ ($x = 0.5, 0.7, 1.0$) samples. The patterns revealed similar structural peaks corresponding to different hexaferrite phases with standard patterns shown in Fig. 2. However, due to the similarity of the structural peaks of the Z-type and Y-type phases, especially the set of peaks in the angular range from 30.25° to 31.1°, the structural phase in a sample was identified by other characteristic structural peaks which exist in the pattern of one phase and not in the other. Specifically, the peaks at $\approx 32.02°$ and 55.0° were used to identify the Y-type phase with standard pattern (JCPDS: 00-044-0207), the peak at 34.65° to identify the W-type phase with the standard pattern (JCPDS: 01-078-0135), and the peaks at 33.3° and 35.0° to identify the Z-type phase with standard pattern (JCPDS: 01-073-2036). The expanded view of the XRD patterns of the samples (Fig. 3) indicated that the Z-type phase was dominant in these samples, whereas the Y-type and W-type phases appeared as secondary phases. The relative intensities of the peaks corresponding to the Y-type phase, however, increased with the increase of x, whereas those corresponding to the W-type phase decreased with the increase of x, and became very weak at $x = 1.0$. This result is consistent with the experimental finding that Zn-containing W-type hexaferrites require higher sintering temperatures (≥ 1300 °C) to stabilize [32–34]. Although the effectiveness of the Zn^{2+} substitution in eliminating the secondary W-type phase from the product is an advantage in the process of Z-type hexagonal ferrite synthesis, the persistence of the Zn_2Y phase is a disadvantage. However, since Zn_2Y and Mg_2Y were reported to be potential materials for multiferroic applications, and possess properties suitable for MLCI and multilayer chip beads [35], the coexisting of the Y-type phase with the Z-type phase in these materials could still be of significant importance for such applications.

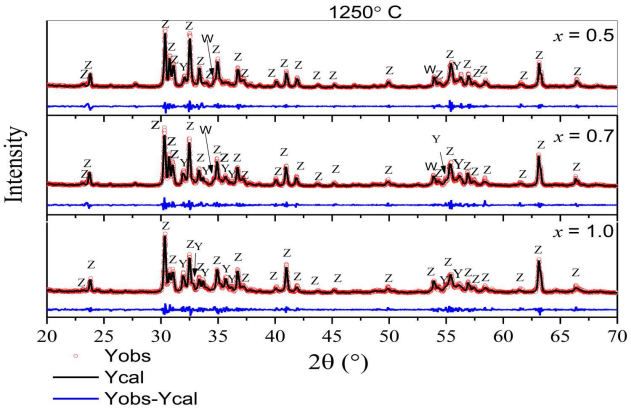

Fig. 1. XRD patterns of $Ba_3(Zn_xMg_{1-x})_2Fe_{24}O_{41}$ samples.

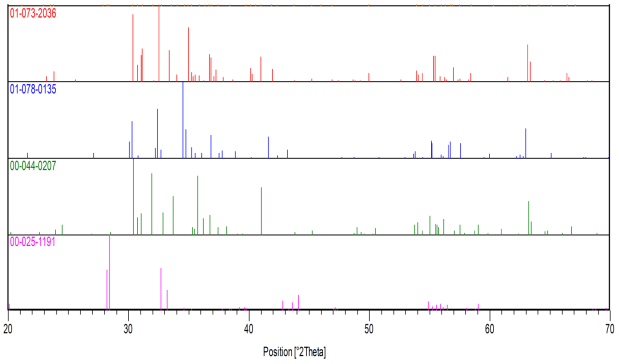

Fig. 2. Standard XRD patterns of Z-, W-, and Y-type hexaferrites as well as that for $BaFe_2O_4$ hexaferrite.

The refined lattice parameters (a and c) and the cell volume V of the hexaferrite phases in the samples were obtained by fitting the XRD patterns using FullProf fitting routine, and the results are listed in Table I. The variations of the lattice parameters with the increase of x were relatively small with no consistent behavior. These variations are reflected as small shifts in the peak positions as Fig. 3 illustrated.

The theoretical X-ray density of each sample was determined using the relation

$$\rho_x = \frac{Z\,(M_w)}{N_A V}. \tag{1}$$

Here Z is the number of molecules per unit cell, M_w is the molecular weight, V is the cell volume, and N_A is Avogadro's number. Also, the bulk densities of

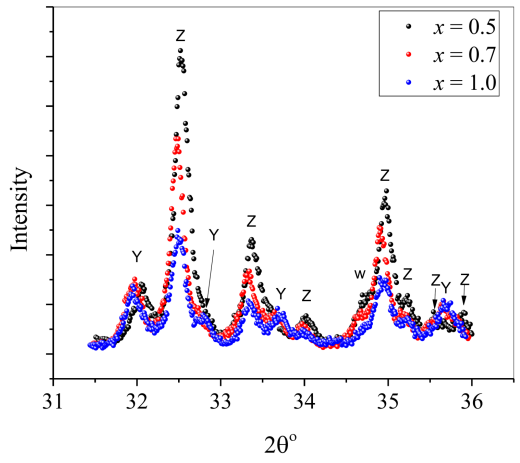

Fig. 3. Expanded view of the diffraction patterns of $Ba_3(Zn_xMg_{1-x})_2Fe_{24}O_{41}$ samples.

TABLE I

Lattice parameter, X-ray density, and bulk density of $Ba_3(Zn_xMg_{1-x})_2Fe_{24}O_{41}$.

x	Phase	a [Å]	c [Å]	V [Å^3]	ρ_x [g/cm^3]	ρ_b [g/cm^3]
0.5	Z	5.89	52.34	1573	5.28	4.56
	Y	5.88	43.59	1307	5.44	
	W	5.90	32.98	994	5.18	
0.7	Z	5.89	52.49	1577	5.29	4.63
	Y	5.89	43.67	1311	5.43	
	W	5.90	33.06	998	5.22	
1.0	Z	5.89	52.35	1573	5.36	4.52
	Y	5.89	43.64	1310	5.43	
	W	5.90	33.02	995	5.28	

the samples were measured using the Archimedes principle, and the results are also presented in Table I. The results indicated that all samples are relatively high density magnets with relative density $\geq 84\%$ (porosity $\leq 16\%$).

The lattice parameter a of the Z-type phase was the same (5.89 Å) for all samples, whereas the lattice parameter c exhibited small fluctuations ($\approx 0.1\%$) around an average value of 52.39 Å, and the cell volume was in the range between 1573 and 1577 Å^3. The refined X-ray density, however, increased systematically from 5.28 g/cm^3 at $x = 0.5$ to 5.36 g/cm^3 at $x = 1.0$, which can be associated with the increase of the molecular mass with the increase of x. Also, the X-ray densities are close to the reported values of 5.37, 5.39, and 5.31 g/cm^3 for Z, Y, and W phases, respectively [36].

3.2. SEM results

The SEM images for the $Ba_3(Zn_xMg_{1-x})_2Fe_{24}O_{41}$ ($x = 0.5$, 0.7, and 1.0) samples are shown in Fig. 4. The image of the sample with $x = 0.5$ (Fig. 4a) showed layered formations which is indicative of topotactical growth [2]. In this formation, crystallization of small (≈ 1 μm) hexagonal crystals was also observed. However, SEM image (Fig. 4c) for sample with $x = 0.7$ revealed crystallization of particles with hexagonal symmetry and few μm in diameter, in addition to large plates (tens of μm in diameter and ≈ 1 μm in thickness as shown in Fig. 4b) which may have evolved through discontinuous grain growth (DGG) process [2]. On the other hand, the sample with $x = 1.0$ was dominated by hexagonal plates with diameters ranging from ≈ 1 to 10 μm (Fig. 4d). The growth of hexagonal platelets on top of each other in a sandwich-like form may indicate that these platelets correspond to different hexaferrite phases observed in XRD measurements (mainly Z-type and Y-type phases).

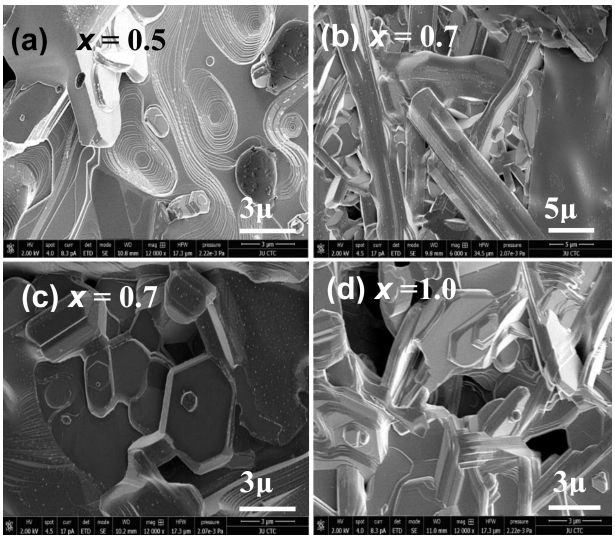

Fig. 4. SEM images for the $Ba_3(Zn_xMg_{1-x})_2Fe_{24}O_{41}$ ($x = 0.5$, 0.7, and 1.0) samples.

3.3. Magnetization measurements

The hysteresis loops of the specific magnetization, σ (emu/g), for $Ba_3(Zn_xMg_{1-x})_2Fe_{24}O_{41}$ samples were measured by VSM at room temperature in an applied field up to 10 kOe. The loops in Fig. 5 were smooth S-shape curves with small coercivity, characteristics of soft magnetic materials. The coercivity of 40 Oe and 43 Oe for the sample with $x = 0.5$ and 0.7, respectively, increased slightly to 54 Oe for the sample with $x = 1.0$ as shown in Table II. Figure 6 shows an expanded view of the hysteresis loops for clarity. The magnetization curves indicated that the saturation magnetization improved with the increase of Zn^{2+} content in the samples. Since the magnetization processes in the high field range are dominated by magnetization rotation of the magnetic domains, the saturation magnetization for the samples was obtained from the law of approach to saturation [37]:

$$M = M_s\left(1 - \frac{A}{H} - \frac{B}{H^2}\right) + \chi H. \qquad (2)$$

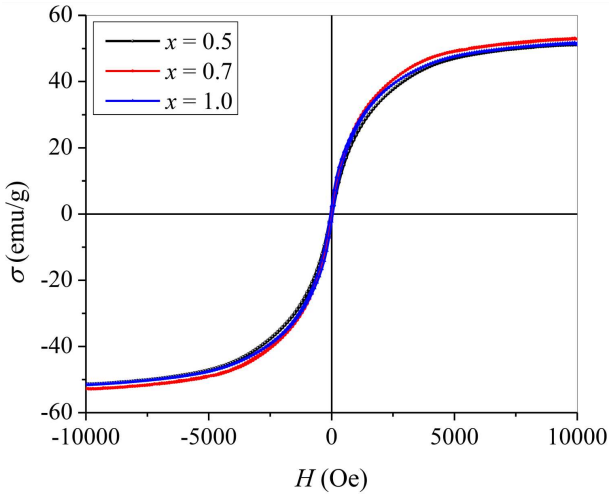

Fig. 5. Hysteresis loops for the $Ba_3(Zn_xMg_{1-x})_2Fe_{24}O_{41}$ samples.

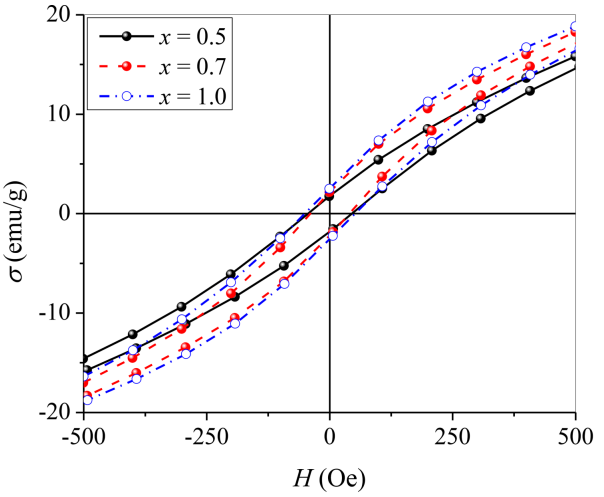

Fig. 6. Expanded view of the hysteresis loops for the $Ba_3(Zn_xMg_{1-x})_2Fe_{24}O_{41}$ samples.

TABLE II

Saturation magnetization σ_s, coercive field H_c, and anisotropy field H_A for the $Ba_3(Zn_xMg_{1-x})_2Fe_{24}O_{41}$ samples.

x	σ_s [emu/g]	H_c [Oe]	H_A [kOe]
0.5	52.8	43	6.8
0.7	54.6	40	6.8
1.0	53.0	54	6.7

Here M_s is the saturation magnetization, A is a constant associated with impurities and crystal imperfections, B is a constant representing the magnetocrystalline anisotropy, and χH is the forced magnetization term. For hexagonal crystals, the constant B is given by [38]:

$$B = \frac{H_A^2}{15}. \tag{3}$$

The specific magnetization σ vs. $1/H^2$ for each sample in the field range of 8 kOe $< H <$ 10 kOe gives a straight line, indicating that the magnetocrystalline anisotropy term dominated the magnetization processes in this field range. The saturation magnetization σ_s, and the anisotropy H_A were determined from the intercept and slope of the straight line as described previously [39], and the results are presented in Table II.

The saturation of all samples is somewhat smaller than the values of 58–59 emu/g reported for Zn_2Z barium hexaferrites [16, 36]. However, the observed values are in agreement with the values recently reported for Zn_2Z hexaferrites [40]. The observed slight reduction of saturation magnetization ($< 10\%$) is associated with the coexistence of Zn_2Y secondary phase with relatively low saturation magnetization of about 35 emu/g [41]. As x is increased, the progressive increase of the relative fraction of the Y-type phase at the expense of the Z-type and W-type phases with higher saturation magnetizations is expected to lower the saturation magnetization. The saturation magnetization, however, increased slightly as x increased. This behaviour is an indication of the effectiveness of Zn^{2+} ionic substitution at spin-down tetrahedral sites in raising the saturation magnetization. On the other hand, the magnetocrystalline anisotropy field (H_A) did not seem to be influenced significantly by the increase of Zn^{2+} content. The observed values of H_A for all samples are higher than the value of 5.6 kOe reported for Zn_2Z hexaferrite [16], but are in good agreement with more recently reported values [40]. In the absence of an applied field, the natural ferromagnetic resonance (FMR) frequency for the uniaxial Z-type hexaferrites in the present study can be estimated by the relation [36]:

$$2\pi f_R = \gamma H_A \rightarrow f_R[\text{MHz}] = 2.80 \times H_A[\text{Oe}]. \tag{4}$$

This relation indicates that the natural ferromagnetic resonance frequency for all samples $f_R \approx 19$ GHz, which is somewhat higher than previously reported observed resonance frequency of 13.4 GHz, or the calculated value (based on Eq. (4)) of 15.7 GHz for Zn_2Z hexaferrite prepared by ball milling and sintering at 1300 °C [16]. On the other hand, these values are much higher than resonance frequencies of < 1 GHz reported for Zn_2Z hexaferrites prepared by sol–gel method [42], which may indicate the sensitivity of the dynamical magnetic properties on the experimental conditions adopted for synthesis of the materials. However, the low resonance frequencies reported in the latter study could be those associated with domain wall motion, whereas natural FMR occurs at a much higher frequencies [16, 36].

Figure 7 shows thermomagnetic curves for the $Ba_3(Zn_xMg_{1-x})_2Fe_{24}O_{41}$ samples at a constants applied field of 100 Oe. The curves revealed three magnetic phase transitions for the three samples, with the Curie temperatures T_C given in Table III. In light of the reported critical transition temperatures [36] of 280 °C, 130 °C, and

360 °C for Mg_2Y, Zn_2Y, and Zn_2Z ferrites, respectively, the first transition (as T is increased) could be associated with Y-type, and the second with Z-type phase. The decrease of the transition temperature of the Y-type phase from 200 °C at $x = 0.5$ to 143 °C at $x = 1.0$ is associated with the increase of Zn^{2+} content in this phase. Also, the increase of the relative height of the first transition step and the decrease of the relative height of the second with increasing x is consistent with the increase of the relative fraction of the Y-type phase and the decrease of the fraction of the Z-type as x is increased. In view of the reported critical temperature in the range 337–407 °C for Zn_2W (depending on the heat treatment) [43], the third transition (at $T > 400$ °C) is attributed to Zn_2W phase. This interpretation is consistent with the decrease of the relative height of the corresponding step as x is increased, which is associated with the progressive decrease of the fraction of the W-type phase as XRD results indicated.

TABLE III

Curie temperatures of the magnetic phases for $Ba_3(Zn_xMg_{1-x})_2Fe_{24}O_{41}$ samples.

x	Curie temperature T_C (±10 °C)		
0.5	200	366	407
0.7	172	366	417
1.0	143	362	419

Assuming that the magnetization processes are determined by rotation of the magnetic domains against the magnetic anisotropy, and ignoring inter-particle interactions, the average value of the initial permeability for a uniaxial polycrystalline sample with randomly oriented crystallites is given by [36]:

$$\mu_i = 1 + \frac{2}{3}\frac{4\pi M_s}{H_A}. \quad (5)$$

Here $M_s = \rho\sigma_s$. Using the values of the saturation magnetization and anisotropy field given in Table II, and the density in Table I, the calculated initial permeability of all samples was almost equal; μ_i (calc.) = 1.31. However, the permeability determined from the measured initial susceptibility ($\mu_i = 1 + 4\pi\chi_i$) was about three times higher as demonstrated by the values of μ_i (obs.) in Table IV. This indicates that domain wall motion has a significant contribution to the initial permeability in our low porosity samples. The multi-domain nature of the particles in our samples was confirmed by SEM imaging, which revealed particle size higher than the critical single domain size of about 0.5 μm [44] for all samples. Also, the results indicated an improvement of the initial permeability with Zn substitution. The observed values of the initial permeability are significantly higher than the value of 2.2 for Zn_2Z hexaferrite, and close to the highest value of 4.0 reported for Co substituted Z-type hexaferrite ($BaCo_xZn_{2-x}O_{41}$) with $x = 0.8$ [16]. However, our results are in agreement with the initial permeability of Zn_2Z hexaferrite prepared by sol–gel method [42].

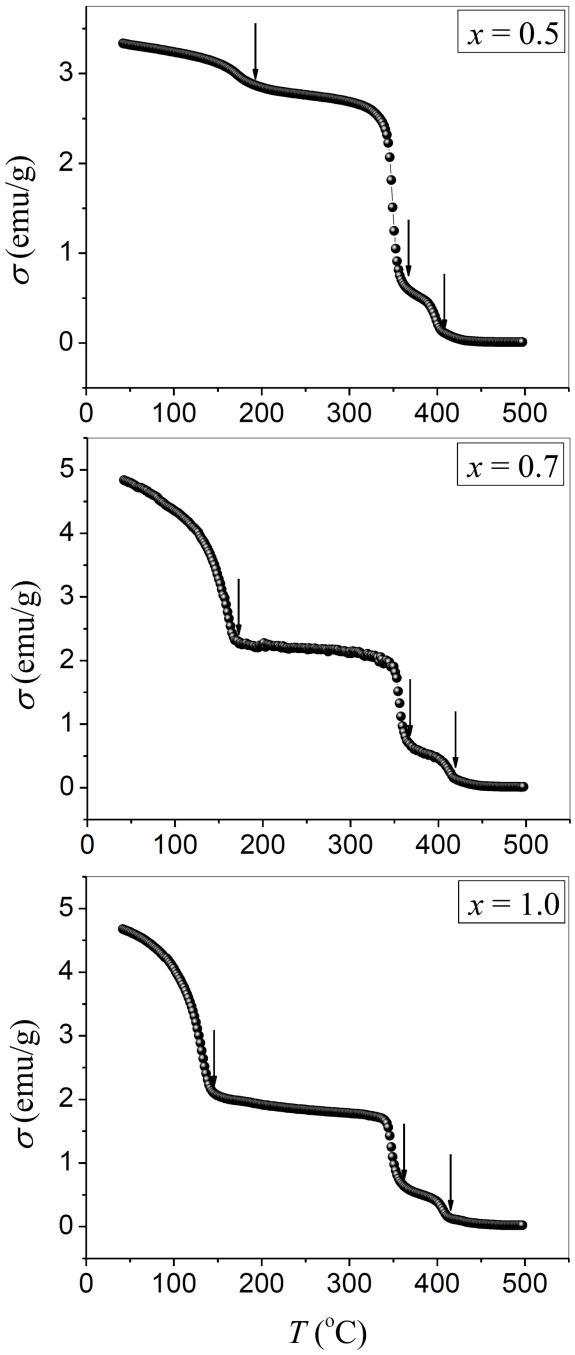

Fig. 7. The $Ba_3(Zn_xMg_{1-x})_2Fe_{24}O_{41}$ thermomagnetic curves at an applied field of 100 Oe. The magnetic phase transition temperatures are indicated by arrows.

TABLE IV

Initial permeability of $Ba_3(Zn_xMg_{1-x})_2Fe_{24}O_{41}$ samples.

x	μ_i (calc.)	μ_i (obs.)
0.5	1.30	3.00
0.7	1.31	3.85
1.0	1.31	3.67

4. Conclusion

Z-type hexaferrite with relatively high purity was prepared by ball milling and sintering at 1250 °C. XRD data indicated that $Ba_3(Zn_xMg_{1-x})_2Fe_{24}O_{41}$ compound with $x = 0.5$ consisted of a major Z-type phase, coexisting with minor Y-type and W-type hexaferrite phases, whereas the increase of Zn content resulted in the increase of the fraction of the Y-type phase and the decrease of the fractions of the Z-type and W-type phases. The presence of these phases was further confirmed by thermomagnetic measurements at low applied magnetic field (100 Oe). Although structurally different, the magnetic parameters of the samples across the substitution range did not change appreciably. Specifically, the saturation magnetization improved only slightly with Zn substitution, whereas the substitution did not seem to have a significant influence on the value of the magnetocrystalline anisotropy field. Also, the FMR frequency estimated from the static magnetic properties suggest that all samples have a natural resonance at around 19 GHz.

However, the Zn substitution had a more pronounced effect on the improvement of the initial permeability, to which domain wall motion contribution seems to be significant.

References

[1] V.G. Harris, A. Geiler, Y. Chen, S.D. Yoon, M. Wu, A. Yang, Z. Chen, P. He, P.V. Parimi, X. Zuo, *J. Magn. Magn. Mater.* **321**, 2035 (2009).

[2] R.C. Pullar, *Progr. Mater. Sci.* **57**, 1191 (2012).

[3] Ü. Özgür, Y. Alivov, H. Morkoç, *J. Mater. Sci. Mater. Electron.* **20**, 789 (2009).

[4] Ü. Özgür, Y. Alivov, H. Morkoç, *J. Mater. Sci. Mater. Electron.* **20**, 911 (2009).

[5] Y. Maswadeh, S.H. Mahmood, A. Awadallah, A.N. Aloqaily, *IOP Conference Series: Materials Science and Engineering*, IOP Publishing, 2015, p. 012019.

[6] S.H. Mahmood, M.D. Zaqsaw, O.E. Mohsen, A. Awadallah, I. Bsoul, M. Awawdeh, Q.I. Mohaidat, *Solid State Phenom.* **241**, 93 (2016).

[7] S.H. Mahmood, in: *Hexaferrite Permanent Magnetic Materials*, Eds. S.H. Mahmood, I. Abu-Aljarayesh, Materials Research Forum LLC, Millersville (PA) 2016, p. 74.

[8] J. Li, H.F. Zhang, G.Q. Shao, D. Chen, G.G. Zhao, Z.S. Gao, J.H. Liu, J.S. Lu, X.B. Li, *Proced. Eng.* **102**, 1885 (2015).

[9] S.H. Mahmood, in Ref. [7], p. 47.

[10] P. Chang, L. He, D. Wei, H. Wang, *J. Europ. Ceram. Soc.* **36**, 2519 (2016).

[11] J. Temuujin, M. Aoyama, M. Senna, T. Masuko, C. Ando, H. Kishi, V. Šepelak, K.D. Becker, *J. Magn. Magn. Mater.* **311**, 724 (2007).

[12] Y. Bai, F. Xu, L. Qiao, J. Zhou, *Mater. Res. Bull.* **44**, 898 (2009).

[13] X. Zhang, Z. Yue, S. Meng, B. Peng, L. Yuan, *Mater. Res. Bull.* **65**, 238 (2015).

[14] X. Wang, L. Li, S. Su, Z. Gui, *J. Am. Ceram. Soc.* **88**, 478 (2005).

[15] J. Wang, A. Geiler, V. Harris, C. Vittoria, *J. Appl. Phys.* **107**, 09A515 (2010).

[16] Z. Li, Y. Wu, G. Lin, L. Chen, *J. Magn. Magn. Mater.* **310**, 145 (2007).

[17] M. Aoyama, J. Temuujin, M. Senna, T. Masuko, C. Ando, H. Kishi, *J. Electroceram.* **17**, 61 (2006).

[18] V.R. Caffarena, J.L. Capitaneo, T. Ogasawara, M.S. Pinho, *Mater. Res.* **11**, 335 (2008).

[19] J. Xu, G. Ji, H. Zou, Y. Zhou, S. Gan, *J. Alloys Comp.* **509**, 4290 (2011).

[20] T. Tachibana, T. Nakagawa, Y. Takada, K. Izumi, T. Yamamoto, T. Shimada, S. Kawano, *J. Magn. Magn. Mater.* **262**, 248 (2003).

[21] R. Pullar, A. Bhattacharya, *Mater. Res. Bull.* **36**, 1531 (2001).

[22] N. Solanki, R.B. Jotania, *Solid State Phenom.* **241**, 226 (2016).

[23] W.H. Dong, H.H. Yong, *Mater. Chem. Phys.* **95**, 248 (2006).

[24] H. Zhang, J. Zhou, Y. Wang, L. Li, Z. Yue, Z. Gui, *Ceram. Int.* **28**, 917 (2002).

[25] H. Zhang, J. Zhou, Y. Wang, L. Li, Z. Yue, X. Wang, Z. Gui, *Mater. Lett.* **56**, 397 (2002).

[26] J. Bao, J. Zhou, Z. Yue, L. Li, Z. Gui, *J. Magn. Magn. Mater.* **250**, 131 (2002).

[27] E.S. Al-Hwaitat, S.H. Mahmood, M.A. Hussein, I. Bsoul, *Adv. Mater. Sci. Eng.* **2018**, 6152020 (2018).

[28] T. Kimura, G. Lawes, A. Ramirez, *Phys. Rev. Lett.* **94**, 137201 (2005).

[29] K. Okumura, K. Haruki, T. Ishikura, S. Hirose, T. Kimura, *Appl. Phys. Lett.* **103**, 032906 (2013).

[30] S.H. Chun, Y.S. Chai, Y.S. Oh, D. Jaiswal-Nagar, S.Y. Haam, I. Kim, B. Lee, D.H. Nam, K.T. Ko, J.H. Park, *Phys. Rev. Lett.* **104**, 037204 (2010).

[31] H. Khanduri, M.C. Dimri, H. Kooskora, I. Heinmaa, G. Viola, H. Ning, M. Reece, J. Krustok, R. Stern, *J. Appl. Phys.* **112**, 073903 (2012).

[32] S. Ram, J.C. Joubert, *J. Magn. Magn. Mater.* **99**, 133 (1991).

[33] A. Paoluzi, F. Licci, O. Moze, G. Turilli, A. Deriu, G. Albanese, E. Calabrese, *J. Appl. Phys.* **63**, 5074 (1988).

[34] A. Pasko, F. Mazaleyrat, M. Lobue, V. Loyau, V. Basso, M. Küpferling, C. Sasso, L. Bessais, *J. Phys. Conf. Series* **303**, 012045 (2011).

[35] Y. Bai, J. Zhou, Z. Gui, Z. Yue, L. Li, *J. Magn. Magn. Mater.* **264**, 44 (2003).

[36] J. Smit, H.P.J. Wijn, *Ferrites*, Wiley, New York 1959.

[37] B.D. Cullity, C.D. Graham, *Introduction to Magnetic Materials*, 2nd ed., Wiley, Hoboken (NJ) 2011.

[38] R. Grössinger, *Phys. Status Solidi A* **66**, 665 (1981).

[39] M. Awawdeh, I. Bsoul, S.H. Mahmood, *J. Alloys Comp.* **585**, 465 (2014).

[40] E.S. Alhwaitat, S.H. Mahmood, M. Al-Hussein, O.E. Mohsen, Y. Maswadeh, I. Bsoul, A. Hammoudeh, *Ceram. Int.* **44**, 779 (2018).

[41] I. Odeh, H.M. El Ghanem, S.H. Mahmood, S. Azzam, I. Bsoul, A.F. Lehlooh, *Physica B* **494**, 33 (2016).

[42] H. Zhang, X. Yao, M. Wu, L. Zhang, *Brit. Ceram. Trans.* **102**, 10 (2003).

[43] G. Litsardakis, D. Samaras, A. Collomb, *J. Magn. Magn. Mater.* **81**, 184 (1989).

[44] L. Rezlescu, E. Rezlescu, P. Popa, N. Rezlescu, *J. Magn. Magn. Mater.* **193**, 288 (1999).